Polarization-controllable TE$_{21}$ mode converter

T. H. Chang, C. F. Yu, and C. T. Fan
Department of Physics, National Tsing Hua University, Hsinchu, Taiwan

We report the concept and development of a Ka-band mode and polarization converter that efficiently converts a TE$_{10}$ rectangular waveguide mode into either a linearly or a circularly polarized TE$_{21}$ cylindrical waveguide mode. The converter is composed of a power-dividing section, a mode-converting section, and a polarization-transitioning section. The converting process in each section is displayed and the working principles are discussed. A prototype has been built and tested. The measured results agree well with the numerical calculations for both linear and circular polarizations. The measured optimum back-to-back transmission is 94% with a 1-dB bandwidth of 4.1 GHz for the linear polarization. As for the circular polarization, the measured optimum transmission is 97%, but the corresponding bandwidth is indistinct due to some resonant dips. The reasons and impact for the dips are discussed. A bandwidth of 3.9 GHz is obtained for a single circular converter; meanwhile, an approach to eliminating these unwanted dips is presented in theory. For further diagnostics, the field pattern of either polarization is directly displayed on a temperature-sensitive liquid crystal display sheet, where the electric field strength can be discerned from the color spectrum. In addition to high conversion efficiency and broad bandwidth, this converter features easy construction, high mode purity, and polarization controllability. © *2005 American Institute of Physics.* [DOI: 10.1063/1.1942528]

I. INTRODUCTION

The TE$_{21}$ mode converter has been employed in a myriad of applications. For example, in the gyrotron application, the second cyclotron harmonic interacting with a TE$_{21}$ waveguide mode is found to have a high-power capability;[1–7] in the microwave/plasma system, a circularly polarized TE$_{21}$ wave is a promising candidate of generating a uniform density plasma with azimuthal symmetry;[8–12] and in the antenna application, the TE$_{21}$ mode antenna can launch and receive differential signals, which produces better directivity.[13,14]

Two methods of generating the TE$_{21}$ mode in a cylindrical waveguide have been proposed. One is the serpentine/corrugated structure,[7,15,16] and the other is the multiholes sidewall coupling.[1,2,5,14,17] The former, using a deformed waveguide structure, gradually converts the wave into the desired mode. The transition length is generally long and multiple modes could be excited during the transition process. The latter generally uses a smooth waveguide with coupling holes on the sidewall. A quad-feed structure is commonly reported. Like the serpentine converter, this type of converter takes up a long converting section, where the modes are gradually settled down to the desired mode. However, the existence of the unwanted modes during the transition could interact with an electron beam, resulting in a serious mode-competition problem for gyrotron applications. Thus, shortening the converting length and enhancing the mode purity help to elude the complicated mode-competition problem.

The cross section of the electric field pattern of the TE$_{21}$ mode has four lobes, each covering a quadrant. The opposing electric field is oriented in the opposite direction. Properly employing this nature can excite a pure TE$_{21}$ mode. Here, we propose a two-port circularly polarized TE$_{21}$ mode converter. A signal is injected into a standard rectangular waveguide port (WR-28, TE$_{10}$ mode) and it is finally converted into a linearly/circularly polarized TE$_{21}$ mode in a cylindrical waveguide.

The rest of this paper is organized as follows. In Sec. II we elaborate on the principle of operation by classifying the converting process into three sections: power-dividing, mode-converting, and polarization-transitioning sections. In Sec. III we detail the design and fabrication considerations. The measured and calculated results are shown in Sec. IV and a direct field pattern measurement is described and displayed in Sec. V.

II. PRINCIPLE OF OPERATION

Figure 1 shows the circular polarization TE$_{21}$ mode converter under study. We divided the converting processes into three stages. The first stage is the power-dividing section, where an input wave at port 1 is divided into two equal amplitudes but opposite-sign signals (180° phase difference). The second stage is the mode-converting section, where the two signals are injected into a cylindrical waveguide to form a pure linearly polarized TE$_{21}$ mode. Finally, the third stage is the polarization-transitioning section, where the just formed linearly polarized TE$_{21}$ wave propagates through a slightly deformed section to form a circularly polarized TE$_{21}$ wave at port 2. The operating principle and design consideration involved in each stage will be discussed in the following.
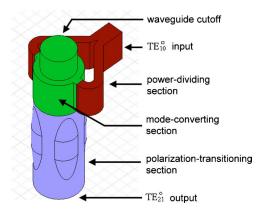
FIG. 1. (Color online) The schematic diagram of the TE_{21} mode and polarization converter under study. The mode-converting processes consist of three stages: the power-dividing section, the mode-converting section, and the polarization-transitioning section.

A. Power-dividing section: Minimizing the input reflection

To compose a TE_{21} mode by using its field property, we generate two equal-amplitude but out of phase signals. A deformed E-plane waveguide Tee provides the desired function. Figure 2 shows the simulation results of the High Frequency Structure Simulator (HFSS, Ansoft). Such a three-port junction cannot be matched simultaneously at all ports, but we can minimize the reflection at the input port (port 1) by optimizing the geometry. Figure 2(a) shows the distribution of the electric field strength of the power dividing section viewed at the middle cross section of the rectangular waveguide. Figure 2(b) plots the reflection at port 1 versus the frequency. Port 1a and port 1b are assumed to be well
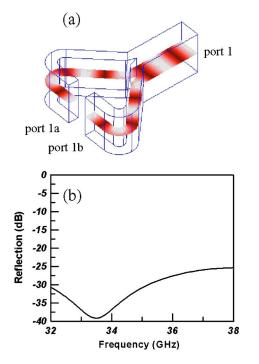

FIG. 2. (Color online) The HFSS simulation results. (a) The distribution of the electric field strength of the power-dividing section, viewed at the middle cross section of the rectangular waveguide. (b) The frequency response of the reflection at port 1, where ports 1a and 1b are assumed to be matched to elude the multiple reflections effect.
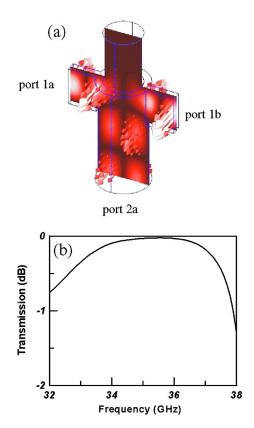

FIG. 3. (Color online) (a) The cross section of the electric field distribution with HFSS. (b) The frequency response of the transmission from two rectangular TE_{10} modes to the circular TE_{21} mode.

terminated to avoid the multiple reflection effect. A broad bandwidth was demonstrated, where the reflection is below 25 dB in this frequency regime.

B. Mode-converting section: Optimizing the transmission

At the end of the first stage, two signals with equal amplitude but opposite sign are generated. In the second stage, these two signals are further worked together to excite a linearly polarized TE_{21} mode. Using the field characteristic of the TE_{21} mode, we can excite the desired mode by injecting the two signals separated by 180° around the circumference. The size of the sidewall apertures is optimized to provide an efficient coupling between the rectangular and cylindrical waveguides. Figure 3(a) shows the cross section of the electric field using HFSS. The waves are injected into both port 1a and port 1b to compose a linearly polarized TE_{21} wave at port 2a.

A microwave short (waveguide cutoff in Fig. 1) is placed at the other end of the cylindrical waveguide. The short is a circular tube with the inner diameter made small enough to completely attenuate the mode of interest and large enough to allow the electron beam to pass through for gyrotron applications. The position of the short affects the center frequency and the bandwidth. Figure 3(b) shows the frequency response of the transmission for a chosen short position. The transmission is obtained using the ratio of the desired power (TE_{21} at port 2a) divided by the total input power (TE_{10} at ports 1a and 1b).
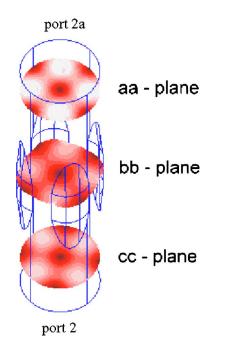
FIG. 4. (Color online) The cross section of the electric field distribution at three different planes: aa plane (linear polarization, before), bb plane (elliptical polarization, middle), and cc plane (circular polarization, after).
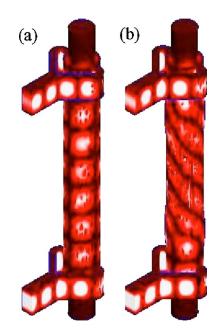

FIG. 5. (Color online) The electric field strengths simulated with HFSS for (a) two identical linearly polarized converters joining back to back, and (b) two identical circularly polarized converters joining back to back.

C. Polarization-transitioning section: Controlling the phase difference

As the linearly polarized TE$_{21}$ wave propagates along the cylindrical waveguide, it enters a polarization-transitioning section with a slight waveguide deformation. Similar to the cylindrical TE$_{11}$ mode, the TE$_{21}$ mode also has two degenerate modes. This property allows us to control its polarization using the same technique developed for the TE$_{11}$ mode converter.[18] The deformed waveguide has two characteristic axes denoted by r_0 and r_1. The two axes are tilted 45° with respect to each other. A linearly polarized TE$_{21}$ wave is decomposed into two equal-amplitude linearly polarized TE$_{21}$ waves. The propagation constant of each wave is characterized by its perspective waveguide radius r_0 or r_1. When the two waves have propagated a distance sufficient to cause a 90° phase difference, the resultant sum of the two waves then becomes a circularly polarized wave. A systematically analysis can be found in Ref. 18.

Figure 4 shows the cross section of the electric field distribution at three different planes: aa plane (linear polarization, before), bb plane (elliptical polarization, middle), and cc plane (circular polarization, after). Note that the field patterns just shown are snapshots. This explains why the circular polarization looks like the linear polarization. In practice, the field pattern of the circular polarization will rotate in time. The polarization could be controlled by properly designing the phase difference. A linearly polarized wave can be restored by simply removing this section.

III. DESIGN AND FABRICATION

Having optimized each section, the next step is to put all the sections together. Using the reciprocity, we can model two identical converters by joining them back to back. The simulation results of the electric field strength are shown in

Fig. 5(a) for two identical linear polarized converters and in Fig. 5(b) for two identical circular polarized converters. We can see that the electric field does not change its polarization for the linearly polarized condition, while the field rotates counterclockwise for the right-hand circular polarization.

Figure 6(a) shows the design of the two identical converters. A circular polarization converter operating at the Ka band is to be built. Part A includes two sections: power dividing and mode converting, where a rectangular TE$_{10}$ mode is converted into a linearly polarized TE$_{21}$ mode in the cylindrical waveguide. Parts B and C are the polarization-transitioning section. One is slightly deformed in the cross section and the other changes back. The tapering angle and the length are optimized with HFSS. The ratio of r_1 to r_0 is designed close to unity to avoid the reflection due to structure nonuniformity, but large enough to maintain a short converting length. A lower r_1/r_0 ratio requires a longer converting section to produce the 90° phase difference between two
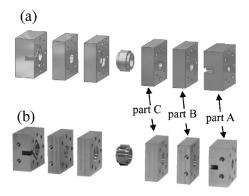

FIG. 6. (a) The design drawing of the parts of the two identical converters. A circular polarization converter operating at the Ka band with a center frequency of 35.0 GHz is to be built. (b) The finished parts, which are made of copper and are machined with a CNC lathe with a tolerance of 0.01 mm. Pins are used to enhance the alignment.
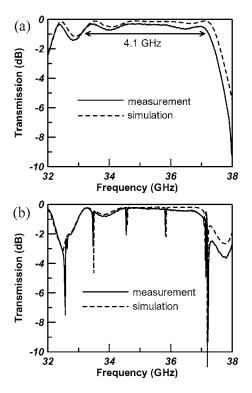
FIG. 7. The calculated and measured transmission loss for two identical converters joining back to back: (a) linear polarization and (b) circular polarization.
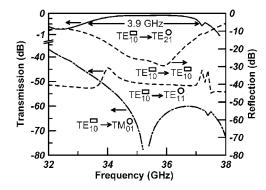

FIG. 8. Calculated transmission loss and reflection loss vs frequency for a single circular polarization mode converter. The transmission loss from a rectangular TE_{10} wave to three cylindrical waveguide modes, TE_{21}, TE_{11}, and TM_{01}, are displayed. The left y axis is broken to display the excellent TE_{21} mode conversion. A 0.5-dB transmission bandwidth is 3.9 GHz.

orthogonal waves. The optimum length has to be determined according to the size constraints and coupling efficiency of the particular application. A compromising design is that the converting section is 2.0 cm long with an average radius of 0.48 cm (r_0) and a maximum deformed radius of 0.53 cm (r_1). A central uniform section of 1.0 cm is used to join the converters together.

Figure 6(b) shows the finished parts. All the parts, made of copper, are machined with a Computer Numerical Control (CNC) lathe with a tolerance of 0.01 mm. Pins are used to ensure the alignment and all the pieces are joined tightly together.

IV. BACK-TO-BACK MEASUREMENT

A back-to-back measurement is commonly used to demonstrate the performance of the coupler. Figures 7(a) and 7(b) show the back-to-back transmission results for linear polarization and circular polarization, respectively. The simulation and measurement setups are similar to Figs. 5, except the center uniform length is only 1.0 cm. A two-port vector network analyzer (VNA, Agilent 8510C) is used to conduct the measurement. For both linear and circular polarization conditions, the measured results show excellent agreement with simulation results. The calculated result shows the conversion loss principally comes from the Ohmic dissipation on the copper walls. The optimum back-to-back conversion efficiency is 94% for the linear polarization case [Fig. 7(a)] with a 1-dB bandwidth of 4.1 GHz (11.7%). However, for the circular polarization case [Fig. 7(b)], the conversion efficiency is even better at the central frequency (97%), but some dips (at 33.6, 34.5, and 35.9 GHz) spoil the

flatness. The back-to-back technique is convenient but is known to create some spurious effect that might not be a problem for a single converter. Moreover, in many applications only a single converter is employed or considered. It is useful to explore the conversion efficiency and mode purity of a single converter.

Figure 8 shows the calculated conversion efficiency and the reflection versus the frequency for a single circular polarization TE_{21} converter. A rectangular TE_{10} wave injecting into port 1 is converted into three cylindrical waveguide modes at port 2, the desired TE_{21} mode as well as the undesired TE_{11} and TM_{01} modes. The conversion efficiency is defined as the power ratio between the output wave in the cylindrical waveguide mode and the input wave in the rectangular TE_{10} mode. The calculated optimum conversion efficiency is 99% with a 0.5 dB bandwidth of 3.9 GHz. The transmission results demonstrate extremely high mode purity (up to 99.99%). The reflection at port 1 is also shown. Excellent agreement for the back-to-back calculated and measured results allows us to have confidence in these simulation results.

Figure 9 presents a simple way to eliminate the dips. An extra port (for example, port A) is added at the sidewall to terminate the degenerate TE_{21} wave due to multiple reflections. The calculated 1-dB back-to-back transmission band-
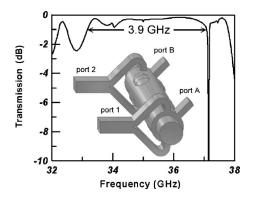

FIG. 9. Calculated back-to-back transmission with extra ports (ports A and B). These extra ports are used to absorb the degenerate TE_{21} wave. The calculated 1-dB bandwidth is 3.9 GHz, which is the same as the single converter's prediction.
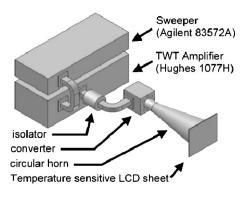
FIG. 10. The schematic diagram of the experimental setup of directly measuring the field distribution pattern. The rf power, generated by a TWT and controlled by a sweeper/synchronizer, is injected into the mode converter. A sheet of temperature-sensitive LCD is placed in front of the circular horn, where the color spectrum is proportional to the electric field strength.

FIG. 11. (Color online) The measured time-averaged field distribution on the LCD sheet for (a) a linearly polarized TE$_{21}$ wave, and (b) a circularly polarized TE$_{21}$ wave.

width is 3.9 GHz, which is the same as the single converter's prediction. Although using this technique could effectively suppress the spurious dips, it degrades the mode purity (from 99.99% to 99.96%) due to asymmetric geometry. For the gyrotron applications, enhancing the mode purity could alleviate the tough mode-competition problem. Thus, whether or not to add the extra port totally depends on the purpose of the application.

Although the back-to-back simulated and measured results agree well, we still need further evidence to show the effectiveness of the converter. One way of doing it is to display the field pattern of TE$_{21}$.

V. FIELD DISTRIBUTION MEASUREMENT

Figure 10 shows the schematic diagram of the experimental setup used to illustrate the field distribution. The rf power of 2 W is provided by a travel wave amplifier (Hughes 1077H), where the frequency is adjusted by a sweeper/synchronizer (Agilent 83572A). A temperature-sensitive liquid crystal display (LCD) sheet, which absorbs microwave energy to raise the local temperature, is placed in front of the circular horn. The LCD sheet displays the full color spectrum in a temperature range of 25–30 °C. The color spectrum displayed on the sheet corresponds to the field energy distribution. This makes us visualize the field pattern directly.

Figure 11 shows the measured results of the time-averaged field strength. Figure 11(a) displays a linearly polarized TE$_{21}$ wave, where the field pattern has four peaks, each occupying a quadrant. For a circular polarized TE$_{21}$ wave, the field pattern rotates in time with a frequency the same as the wave frequency. Only the time-averaged effect will be shown on the LCD sheet. Figure 11(b) illustrates the circular polarized field distribution pattern. The azimuthal symmetric field pattern evidences the mode purity and circular polarization.

In summary, a high-performance TE$_{21}$ mode converter has been proposed, fabricated, and tested. This converter features short converting length ($\sim$1.5 λ_g), high mode purity, high converting efficiency, and polarization controllability. The measured 1-dB transmission bandwidth is 4.1 GHz (11.7%) for the linear polarization and a calculated bandwidth of 3.9 GHz (11.1%) is obtained in theory for the cir-
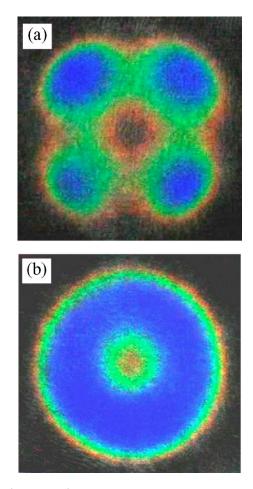
cular polarization. A solution to eliminate the unwanted dips is proposed and verified in theory. With this mode converter, many previously unattainable experiments could be conducted, for example, a second harmonic TE$_{21}$ gyrotron backward-wave oscillator (gyro-BWO) and a second harmonic TE$_{21}$ gyrotron traveling-wave tube amplifier (gyro-TWT).

[1] Q. S. Wang, D. B. McDermott, and N. C. Luhmann, Jr., IEEE Trans. Plasma Sci. **24**, 700 (1996).
[2] Q. S. Wang, D. B. McDermott, and N. C. Luhmann, Jr., Phys. Rev. Lett. **75**, 4322 (1995).
[3] S. J. Cooke, A. W. Cross, W. He, and A. D. R. Phelps, Phys. Rev. Lett. **77**, 4836 (1996).
[4] V. L. Bratman, A. E. Fedotov, Y. K. Kalynov, V. N. Manuilov, M. M. Ofitserov, S. V. Samsonov, and A. V. Savilov, IEEE Trans. Plasma Sci. **27**, 456 (1999).
[5] H. B. Harriet, D. B. McDermott, D. A. Gallagher, and N. C. Luhmann, Jr., IEEE Trans. Plasma Sci. **30**, 909 (2002).
[6] Y. S. Yeh, T. H. Chang, and T. S. Wu, Phys. Plasmas **11**, 4547 (2004).
[7] W. Lawson, M. R. Arjona, B. P. Hogan, and R. L. Ives, IEEE Trans.

Microwave Theory Tech. **48**, 809 (2000).

[8] M. A. Lieberman and R. A. Gottscho, *Physics of Thin Film*, edited by M. H. Francome and J. L. Vossen (Academic, New York, 1994), pp. 25–40.

[9] J. E. Stevens, J. L. Cecchi, Y. C. Huang, and R. L. Jarecki, J. Vac. Sci. Technol. A **9**, 696 (1991).

[10] O. A. Popov, J. Vac. Sci. Technol. A **8**, 2909 (1990).

[11] S. Samukawa, J. Vac. Sci. Technol. A **11**, 2572 (1993).

[12] A. Vegas, M. A. G. Calderon, and E. G. Bustamante, Plasma Phys. Controlled Fusion **26**, 1579 (1984).

[13] V. Y. Lo, TDA Progress Report, 1996, Vol. 42, 104.

[14] Y. H. Choung, K. R. Goudey, and L. G. Bryans, IEEE Trans. Microwave

Theory Tech. **30**, 1862 (1982).

[15] D. B. McDermott, J. Petterebner, C. K. Chong, C. F. Kinney, M. M. Razeghi, and N. C. Luhmann, Jr., IEEE Trans. Microwave Theory Tech. **44**, 311 (1996),

[16] P. J. Clarricoats and A. D. Olver, *Corrugated Horns for Microwave Antennas* (Peter Peregrinus, London, 1984).

[17] F. Sporleder and H. G. Unger, *Waveguide Tapers Transitions and Couplers* (Peter Peregrinus, New York, 1979), Chap. 8.

[18] T. H. Chang, L. R. Barnett, K. R. Chu, F. Tai, and C. L. Hsu, Rev. Sci. Instrum. **70**, 1530 (1999).